ARTICLE

Chinese Journal of Structural Chemistry

Coordination Assembly of Tetrahedral Ti_4(embonate)$_6$ Cages with Alkaline-Earth Metal Ions

Ruiyan Chen[1,2], Guanghui Chen[2], Yanping He[2]* and Jian Zhang[2]*

[1]*College of Chemistry and Materials Science, Fujian Normal University, Fuzhou 350007, China*

[2]*State Key Laboratory of Structural Chemistry, Fujian Institute of Research on the Structure of Matter, Chinese Academy of Sciences, Fuzhou 350002, China*

ABSTRACT Recently, the tetrahedral Ti_4L_6 cage (L = embonate) has been applied as the starting material to realize coordination assembly with transition and rare-earth ornoble metal ions through a two-step reaction. In this work, by employing the Ti_4L_6 cages to assemble with alkaline-earth metal ions (such as Mg^{2+}, Ca^{2+} and Ba^{2+}) under different solvothermal conditions, a series of Ti_4L_6-based structures from simple cages to 1D chain, 2D layer and 3D framework have been synthesized and structurally characterized. In addition, thermal stability, phase purity, UV-vis absorption spectrum, the fluorescent and third-order nonlinear-optical properties are also investigated.

Keywords: metal-organic cages, stepwise-assembly, alkaline-earth, structures, nonlinear optics

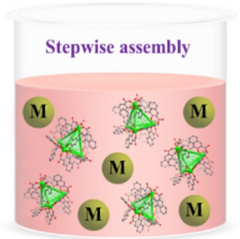

n INTRODUNTION

Compared to other transition metals, alkaline earth metals have some unique advantages for application in materials science such as low cost, low toxicity and high stability in air, etc.[1-3] However, alkaline earth metal-organic frameworks (AE-MOFs) remain largely unexplored due to the inherent difficulties concerning the formation and crystallization of these MOFs.[4-11] Among reported AE-MOFs, many are synthesized by using the carboxylate ligands.[12-17] These AE-MOFs with carboxylate linkers often exhibit high thermal stability because of the strong interaction between alkaline earth metals and carboxylate oxygen atoms, which provides quality assurance for later functional exploration, and is attracting a lot of attention from scientists.[18-21]

In our previous work, we reported an anionic Ti-based cage compound, namely, $[(Me_2NH_2)_8(Ti_4L_6)]$·guests (PTC-101, L = embonate).[22] It is worth pointing out that the Ti_4L_6 cage possesses tetrahedral geometry and calixarene-like coordination-active sites in its each vertex (Figure 1), which has been applied as an especial cage-type carboxylate ligand to realize coordination assembly with transition and rare-earth or noble metal ions through a two-step reaction.[23-27] For example, by employing the Ti_4L_6 cages to assemble with Co or Ln ions, a few architectures with various dimensionalities have been synthesized, including Ti_4L_6-Co3 cage (PTC-103), Ti_4L_6-Ln2 cage (PTC-104), Ti_4L_6-Ln2 chain (PTC-105) and three-dimensional (3D) Ti_4L_6-Ln framework (PTC-106).[22] More interestingly, though introducing the N-contained ligands, two Ti_4L_6-cage-based MOF materials (PTC-219 and PTC-220)[27] have been generated, which show high water stability, thermal stability and notable gas sorption properties.

Herein we investigated the coordination assembly behavior of Ti_4L_6 cages and alkaline-earth metal ions, including Mg^{2+}, Ca^{2+} and Ba^{2+} ions. Under different solvothermal reaction conditions, a series of novel Ti_4L_6-based alkaline-earth complexes with various dimensional architectures have been synthesized (Table 1). Their structures were well characterized by X-ray single crystal diffraction. The thermal stability and phase purity as well as bandgap of these materials were characterized by thermogravimetric analysis (TGA), powder X-ray diffraction (PXRD) and UV-vis absorption spectrum. In addition, we also studied the fluorescent properties of **PTC-306** and **PTC-309** in the solid state, and the results show that both of them display strong emitting bands in the visible region. Furthermore, the results of third-order nonlinear optics[28] show that **PTC-309** exhibits obvious optical limiting effects.

n RESULTS AND DISCUSSION

Synthesis and Structures. At the beginning, $Mg(CH_3COO)_2$ and 4,4'-bipyridine (bpy) were added to the H_2O/THF/EtOH solution of PTC-101, which was heated at 80 °C for three days and then placed at room temperature for a week, forming red polyhedron crystals of **PTC-306**. Single-crystal X-ray diffraction analysis shows **PTC-306** crystallizes in monoclinic space group *C2/c* (Table 1). In the asymmetric unit (Figure S2, ESI), there are a half of Ti_4L_6 cage, one Mg^{2+} ion, five coordinated waters, one free $[Mg(H_2O)_6]^{2+}$ cation, a half of bpy (4,4'-bipyridine) ligand, two $(Me_2NH_2)^+$ cations and some guest molecules (cations and some guest molecules could not be located because of disorder and squeezed by PLATON program). In fact, the starting material PTC-101 is a racemic mixture containing ΔΔΔΔ-$[Ti_4L_6]$ and ΛΛΛΛ-$[Ti_4L_6]$ enantiomers (Figure S1, ESI). In **PTC-306**, the ΔΔΔΔ-$[Ti_4L_6]$ and ΛΛΛΛ-$[Ti_4L_6]$ cages each catch two Mg atoms by two formerly uncoordinated carboxyl oxygen atoms at one vertex of the Ti_4L_6 tetrahedron, and each Mg1 center is six-coordinated by one carboxyl oxygen atom and five water oxygen atoms, forming $[Mg(H_2O)_5]_2$-ΛΛΛΛ-$[Ti_4L_6]$ and $[Mg(H_2O)_5]_2$-ΔΔΔΔ-$[Ti_4L_6]$ cage (Figure 2a), respectively.

Interestingly, the in-situ self-generating $[Mg(H_2O)_6]^{2+}$ cation further connects two $[Mg(H_2O)_5]_2$-ΛΛΛΛ-$[Ti_4L_6]$ cages through multiple O−H···O hydrogen bonds (2.6−3.2 Å) (Figure 2c), generating a 2D H-bonding chiral layer (Figure 2e). Expectedly, the opposite 2D H-bonding chiral layer constructed by the opposite $[Mg(H_2O)_5]_2$-ΔΔΔΔ-$[Ti_4L_6]$ cages and $[Mg(H_2O)_6]^{2+}$ cations can also be observed in **PTC-306** (Figure 2f). The resulting layers further pack into a 3D achiral supramolecular structure in an AB fashion (Figure S3, ESI), and there are strong O−H···O (~2.74 Å) interactions between adjacent layers. It is worth pointing out that all

DOI: 10.14102/j.cnki.0254-5861.2021-0016

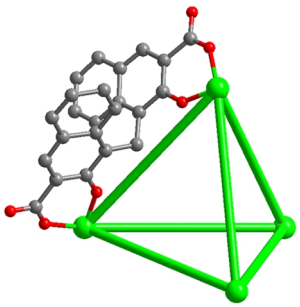

Figure 1. A molecular structure of Ti_4L_6 cage as an organic building block used in the synthesis of this work.

bpy ligands are not involved in the coordination, but are located at the layers by the O−H···N (~2.79 Å) interactions.

The synthetic experiments are still being explored, and the Ba^{2+} ions with high coordination number were used to assemble with Ti_4L_6 cages. In the presence of tris(4-(1H-1,2,4-triazol-1-yl)phenyl)amine (TIPA) ligand, the solvothermal reaction of $BaCl_2$ and PTC-101 in H_2O/DMSO at 80 °C for 3 days yielded compound **PTC-307**. The structural analysis of **PTC-307** shows that it is a chain structure. It crystallizes in the triclinic space group $P\bar{1}$. As shown in Figure S4a (ESI), the asymmetric unit contains one Ti_4L_6 cage, three Ba^{2+} ions, five coordinated H_2O, five coordinated DMSO molecules, one free $[Ba(DMSO)_6]^{2+}$ and two Cl^- counterion anions (solvent guests could not be located because of high disorder and squeezed by PLATON program). Herein, the TIPA ligand is not observed in the structure, and it is only an adjunct to the crystallization. In **PTC-307**, each Ti_4L_6 cage catches three Ba atoms by three uncoordinated carboxyl oxygen atoms at three vertices of the tetrahedron. The Ba1, Ba2 and Ba4 atoms are seven-, eight- and eight-coordinated (Figure S4b, ESI), respectively. Thereinto, Ba1 and Ba2 atoms are bridged by one carboxylate group and two DMSO molecules to form a binuclear $Ba_2(COO)_5(H_2O)_3(DMSO)_4$ unit with the Ba···Ba distance of 4.26 Å, which further links two adjacent Ti_4L_6 cages to form a linear Ti_4L_6-Ba_3 chain. Interestingly, spontaneous resolution occurred during the formation of chain, leading to a chiral chain with only ΛΛΛΛ-[Ti_4L_6] or ΔΔΔΔ-[Ti_4L_6] cages (Figure 3a). These chains further pack into a 3D dense achiral superstructure in an AB stacking order (Figure 3c), in which the free $[Ba(DMSO)_6]^{2+}$ cations are filled in the crack via weak C−H···π (3.3−3.6 Å) interactions. In addition, there are also weak hydrogen bonds (O−H···O: 2.6−3.3 Å; C−H···O: 3.1−3.4 Å) between neighbouring chains (Figures 3d−e and S5).

Table 1. Summary of the Compositions and Characteristics of the Obtained Compounds

Complex	Composition	Space group	Structure dimensionality
PTC-306	$\{(Me_2NH_2)_4[Mg(H_2O)_6]_2$-$[Mg_2(Ti_4L_6)(H_2O)_{10}]\}\cdot$(bpy)	*C*2/*c*	0D
PTC-307	$\{[Ba(DMSO)_6][Ba_4(Ti_4L_6)$-$(H_2O)_8(DMSO)_5]Cl_2\}$	$P\bar{1}$	1D
PTC-308	$\{(Me_4N)_7[Ca_6(Ti_4L_6)_2(OH)_3$-$(H_2O)_{18}(DMF)_3]\}$	$R\bar{3}c$	2D
PTC-309	$\{(Me_2NH_2)_2[Mg_3(Ti_4L_6)$-$(H_2O)_{12}]\}$	$Pa\bar{3}$	3D

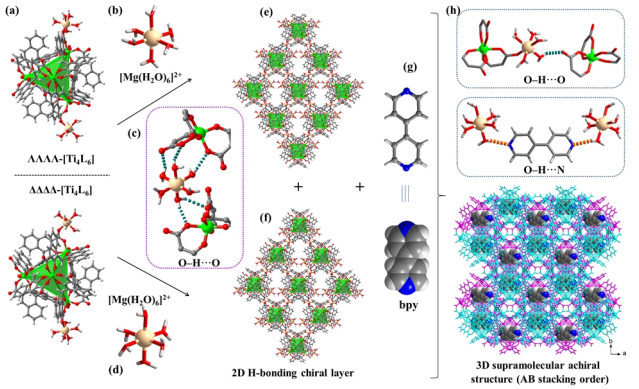

Figure 2. (a) Two configurations of $[Mg(H_2O)_5]_2$-Ti_4L_6 cage in **PTC-306**; (b, d) the free $[Mg(H_2O)_6]^{2+}$ cation; (c) highlighting of the O−H···O hydrogen bonds in **PTC-306**; (e, f) the 2D H-bonding chiral layer; (g) the free bpy ligand; (h) the 3D supramolecular structure of **PTC-306** and some relevant hydrogen bonds. Atom color code: green, Ti; carnatio, Mg; red, O; blue, N; gray, C; offwhite, H.

Moreover, we also studied the assembly behavior of Ti_4L_6 cages with Ca^{2+} ions. Through the solvothermal reaction of $CaCl_2$ and PTC-101 in the presence of tetramethylammonium bromide (Me_4NBr), red block crystals of **PTC-308** were obtained. Structure

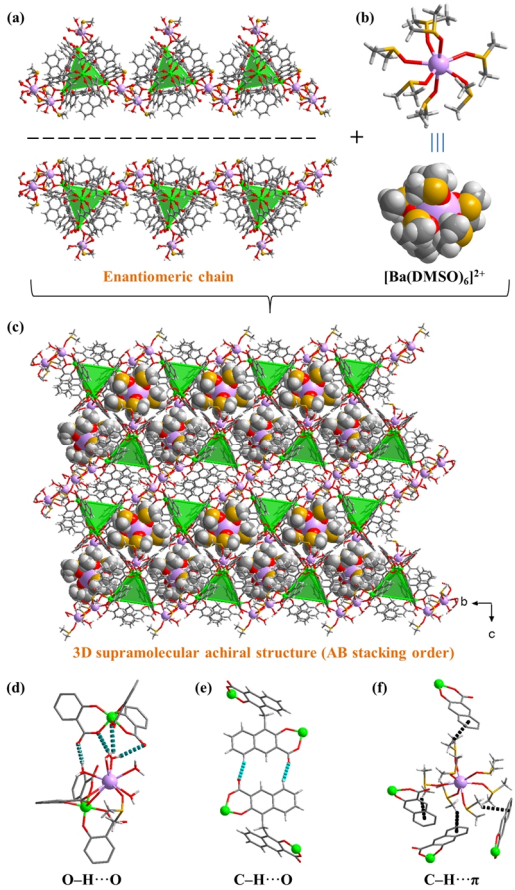

Figure 3. (a) The enantiomeric chain in **PTC-307**; (b) the free $[Ba(DMSO)_6]^{2+}$ cation; (c) the 3D supramolecular structure; (d−f) highlighting of the hydrogen bonds in **PTC-307**. Atom color code: green, Ti; mauve, Ba; red, O; blue, N; gray, C; offwhite, H.

DOI: 10.14102/j.cnki.0254-5861.2021-0016

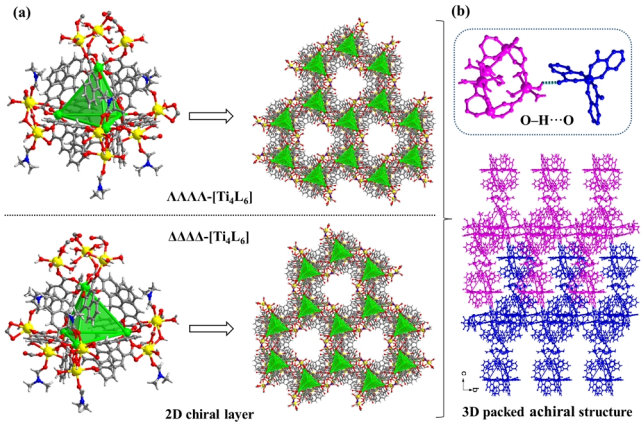

Figure 4. (a) The 2D chiral layers constructed by the ΛΛΛΛ-[Ti_4L_6] or ΔΔΔΔ-[Ti_4L_6] cages and Ca^{2+} ions in **PTC-308**; (b) packed layers of **PTC-308** and the O−H···O hydrogen bonds between adjacent layers.

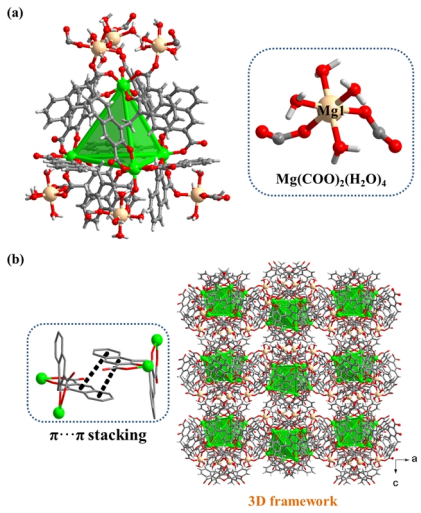

Figure 5. (a) The coordination environments of Ti_4L_6 cage and Mg^{2+} atom in **PTC-309**; (b) the 3D framework and the $\pi\cdots\pi$ stacking interactions between adjacent naphthalene rings in **PTC-309**.

determination indicates that **PTC-308** is a 2D layer with honeycomb-like structure. It crystallizes in the trigonal space group *R*3*c*. As shown in Figure 4a, each Ti_4L_6 cage catches nine Ca atoms by the formerly uncoordinated carboxyl oxygen atoms. Ca2 center with four coordinated H_2O is six-coordinated to form a mononuclear $Ca(COO)_2(H_2O)_4$ unit (Figure S6, ESI). While Ca1 center is seven-coordinated, and a pair of Ca1 atoms are bridged by two μ2-OH^- groups to generate a dinuclear $Ca_2(OH)_2(COO)_4(H_2O)_2$-$(DMF)_2$ unit with Ca···Ca distance of 4.43 Å. Two types of building units connect Ti_4L_6 cages to generate a 2D Ti_4L_6-Ca_3 layer structure with honeycomb-like channels. Surprisingly, spontaneous resolution also occurred during formation of layer herein, leading to a chiral layer with only ΛΛΛΛ-[Ti_4L_6] or ΔΔΔΔ-[Ti_4L_6] cages (Figure 4a). Such a pair of chiral layers further packs into a 3D dense achiral superstructure in an AB stacking order (Figures 4b and S7), and adjacent layers are stabilized by the strong O–H···O (~2.76 Å) hydrogen bonds.

However, in the absence of bpy ligand, when the reaction solvent of **PTC-306** was changed to H_2O/CH_3CN, a 3D Ti_4L_6-Mg-based framework (**PTC-309**) was generated. Single-crystal structural analysis reveals that **PTC-309** crystallizes in a highly symmetric cubic crystal system with space group *Pa*$\bar{3}$. The asymmetric unit of **PTC-309** contains one third of Ti_4L_6 cage, one Mg^{2+} ion, four coordinated H_2O molecules and the free $(Me_2NH_2)^+$ cations which could not be located because of high disorder (Figure S8, ESI). In **PTC-309**, each Mg center is six-coordinated to two carboxylate oxygen atoms from two Ti_4L_6 cages and four terminal water molecules, forming a mononuclear $Mg(COO)_2(H_2O)_4$ unit. Each Ti_4L_6 cage captures six Mg atoms by the formerly uncoordinated carboxyl oxygen atoms at four vertexes of the tetrahedron (Figure 5a). Such connectivity between mononuclear $Mg(COO)_2(H_2O)_4$ units with Ti_4L_6 cages generates an anionic 3D framework with small channels at the b-axis (Figure 5b). In addition, there are rich weak $\pi\cdots\pi$ stacking (3.9−4.1 Å) interactions between adjacent naphthalene rings of two different Ti_4L_6 cages. Calculated by the PLATON program, the free space in the structure of **PTC-309** without guest molecules and $(Me_2NH_2)^+$ cantions is about 36%.

Thermal Stability, Phase Purity and Bandgaps. The thermal stability and phase purity of these compounds were studied by the thermogravimetric analyses (TGA) and X-ray powder diffraction (PXRD). As shown in Figures S9 to S11 (ESI), the TGA curves of **PTC-306** and **PTC-309** reveal a weight loss of 17.5% and 19.6% before 200 °C, respectively, and **PTC-307** shows two steps of weight loss process between 20 and 400 °C, which are related to the removal of free solvents and coordinated solvent molecules. As temperatures rise, their supramolecular or 3D frameworks begin to collapse. After decomposition, the residue of them may be TiO_2 and MgO or CaO. The PXRD patterns demonstrated the phase purity of their samples (Figures S12 to S14, ESI), because

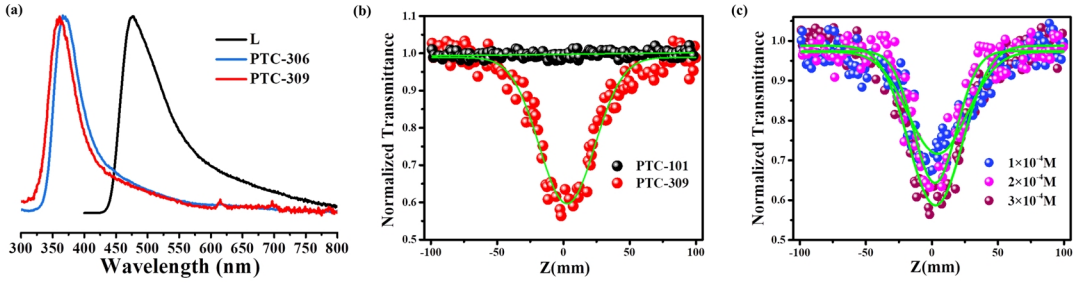

Figure 6. (a) Normalized emission spectra measured in air at room temperature for the L ligand and compounds **PTC-306** and **PTC-309**; (b) OA Z-scan (points) and theoretical fit (solid lines) curves of **PTC-101** and **PTC-309** at 532 nm and different concentrations of **PTC-309** (c).

DOI: 10.14102/j.cnki.0254-5861.2021-0016

their patterns are quite similar to the one simulated from their single-crystal data. In addition, electronic properties of these materials were also investigated using UV-vis diffuse reflectance spectroscopy. The results show that the bandgaps of **PTC-306** and **PTC-309** are 1.89 and 1.87 eV (Figure S15, ESI), respectively, which are calculated by the Kubelka-Munk function, and exhibit relatively lower bandgap than PTC-101 (1.91 eV). For **PTC-307**, we did not study any property because of the low yield.

Fluorescence. The solid-state excitation and emission spectra of compound **PTC-306** and **PTC-309** as well as the free embonate (L) ligand were recorded at room temperature. As shown in Figure 6a, the highly π-conjugated organic L ligand exhibits an emission band at 476 nm upon excitation at 360 nm (Figure S16, ESI), which can be assigned to the $\pi \rightarrow \pi^*$ transition. The emissions of **PTC-306** and **PTC-309** have patterns similar to that of the free ligand with maximum absorption emission band at around 359 and 367 nm, respectively. But by contrast, they are all blue-shifted more than 110 nm. Their excitation spectra are shown in Figures S17–18. Obviously, the ligand-based luminescence is in a dominating place herein, and the blue-shifted phenomenon may be attributed to the metal-ligand coordinative interactions.

Nonlinear Optics. Furthermore, based on the rich $\pi\cdots\pi$ interactions between adjacent naphthalene rings in **PTC-309**, we decided to study its third-order NLO property. The open aperture (OA) Z-scan measurement was carried out for its CH_2Cl_2 solutions (3×10^{-4} M). As shown in Figure 6b, the recorded OA Z-scan curve of **PTC-309** displays distinct reverse saturated absorption (RSA) behaviour. As a contrast, the optical limiting property of the starting material PTC-101 was also measured. The test result reveals that PTC-101 does not have obvious light-limiting effect, which further explains that **PTC-309** presents significantly optical limiting property under 532 nm, mainly attributed to the abundant $\pi\cdots\pi$ stacking interactions in the structure. Additionally, we also studied the effect of concentration on the optical limiting performance (Figure 6c). The experiment result indicates that the opting effects of **PTC-309** are not explicitly dependent on its concentration.

n CONCLUSION

In summary, we have investigated the coordination assembly behavior of Ti_4L_6 cages and alkaline-earth metal ions (such as Mg^{2+}, Ca^{2+} and Ba^{2+}) herein, respectively. Under different solvothermal conditions, a series of novel Ti_4L_6-based structures from simple cages to 1D chain, 2D layer and 3D framework have been synthesized and structurally characterized, respectively. **PTC-306** and **PTC-309** exhibit strong emitting bands in the visible region. Moreover, we demonstrate that **PTC-309** has obvious optical limiting effect because of weak $\pi\cdots\pi$ stacking interactions between L ligands from adjacent cages.

n EXPERIMENTAL

Materials and Methods. All reagents were purchased commercially and used without further purification. PTC-101 as a starting material of $Ti_4L_{6\ cage}$s was massively synthesized by the method reported in our previous work.[21] Thermal stability studies were carried out on a NETSCHZ STA-449C thermoanalyzer with a heating rate of 10 °C/min under a nitrogen atmosphere. Powder XRD was recorded on a Rigaku Dmax/2500 X-ray diffractometer operating at 40 kV and 100 mA, using Ga-Kα or Mo-Kα radiation (λ = 1.3405 or 0.71073 Å). The patterns were scanned over an angular range of 3–45° (2theta) with a step length of 0.05° (2theta). The UV diffuse reflection data were recorded at room temperature using a powder sample with $BaSO_4$ as a standard (100% reflectance) on a PerkinElmer Lamda-950 UV spectrophotometer. Fluorescence spectra were measured with a HORIBA Jobin-Yvon FluoroMax-4 spectrometer.

Synthesis of $\{(Me_2NH_2)_4[Mg(H_2O)_6]_2[Mg_2(Ti_4L_6)(H_2O)_{10}]\}\cdot$(bpy)$\cdot$*guests* (PTC-306). PTC-101 (80 mg, 0.02 mmol), 4,4'-bipyridine (bpy) (20 mg, 0.13 mmol) and $Mg(CH_3COO)_2$ (40 mg, 0.28 mmol) were dissolved in 6 mL of H_2O/THF/EtOH (1:1:1, v/v/v) mixed solvents. The mixture was heated at 80 °C for 3 days, and then placed at room temperature for 1 week. Red polyhedron crystals of **PTC-306** were obtained. Yield: 63% based on PTC-101.

Synthesis of $\{[Ba(DMSO)_6][Ba_4(Ti_4L_6)(H_2O)_8(DMSO)_5]Cl_2\}\cdot$*guests* (PTC-307). PTC-101 (80 mg, 0.02 mmol), tris(4-(1H-1,2,4-triazol-1-yl)phenyl)amine (TIPA) (30 mg, 0.07 mmol) and $BaCl_2$ (30 mg, 0.14 mmol) were dissolved in 6 mL of H_2O/DMSO (1:2, v/v; DMSO = dimethyl sulfoxide) mixed solvents. The mixture was heated at 80 °C for 3 days, and then placed at room temperature for 1 week, obtaining red polyhedron crystals of **PTC-307** in 8% yield based on PTC-101.

Synthesis of $\{(Me_4N)_7[Ca_6(Ti_4L_6)_2(OH)_3(H_2O)_{18}(DMF)_3]\}\cdot$*guests* (PTC-308). PTC-101 (80 mg, 0.02 mmol), $CaCl_2$ (30 mg, 0.27 mmol) and tetramethylammonium bromidewere (30 mg, 0.20 mmol) dissolved in 5 mL of H_2O/DMF (3:2, v/v) mixed solvents. The mixture was placed at room temperature for 1 week, and red block crystals of **PTC-308** were obtained. Yield: 55% based on PTC-101.

Synthesis of $\{(Me_2NH_2)_2[Mg_3(Ti_4L_6)(H_2O)_{12}]\}\cdot$*guests* (PTC-309). PTC-101 (80 mg, 0.02 mmol) and $Mg(CH_3COO)_2$ (40 mg, 0.28 mmol) were dissolved in 6 mL of H_2O/CH_3CN (1:2, v/v) mixed solvents. After the mixture was heated at 80 °C for 3 days, red block crystals of **PTC-309** were obtained. Yield: 78% based on PTC-101.

X-ray Structure Determination. Crystallographic data of **PTC-306** to **PTC-309** were collected on a Supernova single crystal diffractometer equipped with graphite-monochromatic Ga-Kα or Mo-Kα radiation (λ = 1.3405 or 0.71073 Å) at 100 K. Absorption correction was applied using SADABS. Structure was solved by direct method and refined by full-matrix least-squares on F^2 using SHELXTL. In these structures, some cations/anions and free guest molecules were highly disordered and could not be located. The diffused electron densities resulting from these residual cations/anions and guest molecules were removed from the data set using the SQUEEZE routine of PLATON and refined further using the data generated. Crystal data and details of data collection and refinement of **PTC-306** to **PTC-309** were summarized in Table S1. CCDC 2108023−2108026 contain the supplementary crystallographic data for this paper. These data are provided free of charge by the Cambridge Crystallographic Data Centre.

Nonlinear Optics. The nonlinear optical property of **PTC-309** was evaluated using the open-aperture (OA) Z-scan technique. The excitation light source was an Nd:YAG laser with a repetition rate of 10 Hz. The laser pulses (period, 8.5 ns; wavelength, 532 nm)

DOI: 10.14102/j.cnki.0254-5861.2021-0016

were split into two beams with a mirror. The pulse energies at the front and back of the samples were monitored using energy detectors D1 and D2. All of the measurements were conducted at room temperature. Crystals of **PTC-309** were dispersed in CH_2Cl_2 (3×10^{-4} M). The sample was mounted on a computer-controlled translation stage that shifted each sample along the z-axis. Moreover, the optical-limiting effects of **PTC-309** are almost linearly dependent on its concentration, and the NLO response increases with an increase in the concentration.

n ACKNOWLEDGEMENTS

This work is supported by National Natural Science Foundation of China (21773242 and 21935010).

n AUTHOR INFORMATION

Corresponding authors. E-mail: hyp041@163.com and zhj@fjirsm.ac.cn

n COMPETING INTERESTS

The authors declare no competing interests.

n ADDITIONAL INFORMATION

Supplementary information is available for this paper at http://manu30.matech.com.cn/jghx/EN/10.14102/j.cnki.0254-5861.2021-0016

For submission: https://mc03.manuscriptcentral.com/cjsc

n REFERENCES

(1) Zang, Y.; Li, L. K.; Zang, S. Q. Recent development on the alkaline earth MOFs (AEMOFs). *Coord. Chem. Revs.* **2021**, 440, 213955–213983.

(2) Liu, K.; Xu, X.; Xu, J.; Fang, X.; Liu, L.; Wang, X. The distributions of alkaline earth metal oxides and their promotional effects on Ni/CeO_2 for CO_2 methanation. *Journal of CO_2 Utilization* **2020**, 38, 113–124.

(3) Liu, C. H.; Fang, W. H.; Kang, Y.; Zhang, J. Synthetic strategies, diverse structures and properties of copper halide cluster-based materials. *Chin. J. Struct. Chem.* **2021**, 39, 2091–2101.

(4) Hu, J.; Liu, Y.; Liu, J.; Gu, C. Computational screening of alkali, alkaline earth, and transition metals alkoxide-functionalized metal-organic frameworks for CO_2 capture. *J. Phys. Chem. C* **2018**, 122, 19015–19024.

(5) Yao, J.; Liu, Y. E.; Yang, L. B.; Dou, A. N.; Hou, C. F.; Xu, Q. Q.; Huang, B.; Zhu, A. X. Novel alkaline earth metal-organic frameworks with thiophene groups for selective detection of Fe^{3+}. *CrystEngComm*. **2020**, 22, 5970–5979.

(6) Guo, S. S.; Huang, L. L.; Ye, Y. X.; Liu, L. Z.; Yao, Z. Z.; Xiang, S. C.; Zhang, J. D.; Zhang, Z. J. Carbazole based anionic MOF for proton conductivity. *Chin. J. Struct. Chem.* **2021**, 40, 55–60.

(7) Asgharnejad, L.; Abbasi, A.; Najafi, M.; Janczak, J. Synthesis and structure of three new alkaline earth metal-organic frameworks with high thermal stability as catalysts for knoevenagel condensation. *Cryst. Growth Des*. **2019**, 19, 2679–2686.

(8) Matlinska, M. A.; Ha, M.; Hughton, B.; Oliynyk, A. O.; Iyer, A. K.; Bernard, G. M.; Lambkin, G.; Lawrence, M. C.; Katz, M. J.; Mar, A.; Michaelis, V. K. Alkaline earth metal-organic frameworks with tailorable ion release: a path for supporting biomineralization. *ACS Appl. Mater. Interfaces.* **2019**, 11, 32739–32745.

(9) Hou, Y.; Liu, L.; Zhang, Z.; Sun, J.; Zhang, Y.; Jiang, J. Synthesis, crystal structures, and fluorescence properties of porphyrin alkaline earth MOFs. *Inorg. Chem. Commun*. **2018**, 95, 36–39.

(10) Hou, Y.; Sun, J.; Zhang, D.; Qi, D.; Jiang, J. Porphyrin-alkaline earth MOFs with the highest adsorption capacity for methylene blue. *Chemistry* **2016**, 22, 6345–6352.

(11) Krieck, S.; Schuler, P.; Gorls, H.; Westerhausen, M. Alkaline-earth metal bis[bis(trimethylsilyl)amide] complexes with weakly coordinating 2,2,5,5-tetramethyltetrahydrofuran ligands. *Inorg. Chem.* **2018**, 57, 13937–13943.

(12) Zhou, X.; Chen, Q.; Li, L.; Yang, T.; Wang, J.; Huang, W. Three alkaline earth metal-organic frameworks based on fluorene-containing carboxylates: syntheses, structures and properties. *Sci. Chin. Chem*. **2016**, 60, 115–121.

(13) Douvali, A.; Papaefstathiou, G. S.; Gullo, M. P.; Barbieri, A.; Tsipis, A. C.; Malliakas, C. D.; Kanatzidis, M. G.; Papadas, I.; Armatas, G. S.; Hatzidimitriou, A. G. Alkaline earth metal ion/dihydroxy-terephthalate MOFs: structural diversity and unusual luminescent properties. *Inorg. Chem*. **2015**, 54, 5813–5826.

(14) Wu, Z. F.; Tan, B.; Lustig, W. P.; Velasco, E.; Wang, H.; Huang, X. Y.; Li, J. Magnesium based coordination polymers: syntheses, structures, properties and applications. *Coord. Chem. Revs*. **2019**, 399, 213025–213051.

(15) Salmeia, K. A.; Dolabella, S.; Parida, D.; Frankcombe, T. J.; Afaneh, A. T.; Cordova, K. E.; Al-Maythalony, B.; Zhao, S.; Civioc, R.; Marashdeh, A. Robust barium phosphonate metal-organic frameworks synthesized under aqueous conditions. *ACS Mater. Lett*. **2021**, 3, 1010–1015.

(16) Li, K.; He, K.; Li, Q.; Xia, B.; Wang, Q.; Zhang, Y. Crystal structure and photoluminescence properties of two barium(II) MOFs. *Chem. Res. Chin. Univ.* **2018**, 34, 700–704.

(17) Kojima, D.; Sanada, T.; Wada, N.; Kojima, K. Synthesis, structure and fluorescence properties of a calcium-based metal-organic framework. *RSC Adv*. **2018**, 8, 31588–31593.

(18) Xu, N.; Zhang, Q.; Hou, B.; Cheng, Q.; Zhang, G. A novel magnesium metal-organic framework as a multiresponsive luminescent sensor for Fe(III) Ions, pesticides, and antibiotics with high selectivity and sensitivity. *Inorg. Chem.* **2018**, 57, 13330–13340.

(19) Pankajakshan, A.; Mandal, S. Water stable boronic acid grafted barium metal-organic framework for the selective adsorption of cis-diols. *Inorg. Chem.* **2020**, 59, 5958–5965.

(20) Wang, X. T.; Wei, W.; Zhang, K.; Du, S. W. Detection of diethyl ether by a europium MOF through fluorescence enhancement. *Chin. J. Struct. Chem.* **2021**, 40, 369–375.

(21) Bazyakina, N. L.; Makarov, V. M.; Ketkov, S. Y.; Bogomyakov, A. S.; Rumyantcev, R. V.; Ovcharenko, V. I.; Fedushkin, I. L. Metal-organic frameworks derived from calcium and strontium complexes of a redox-active ligand. *Inorg. Chem.* **2021**, 60, 3238–3248.

(22) He, Y. P.; Yuan, L. B.; Chen, G. H.; Lin, Q. P.; Wang, F.; Zhang, L.; Zhang, J. Water-soluble and ultrastable Ti_4L_6 tetrahedron with coordination assembly function. *J. Am. Chem. Soc.* **2017**, 139, 16845–16851.

(23) He, Y. P.; Yuan, L. B.; Chen, G. H.; Zhang, L.; Zhang, J. Coordination assembly of the water-soluble $Ti_4(embonate)_6$ cages with Mn^{2+} ions. *Isr. J. Chem.* **2018**, 59, 233–236.

(24) He, Y. P.; Chen, G. H.; Yuan, L. B.; Zhang, L.; Zhang, J. $Ti_4(embonate)_6$ cage-ligand strategy on the construction of metal-organic frameworks with high stability and gas sorption properties. *Inorg. Chem.* **2020**, 59, 964–967.

(25) He, Y. P.; Chen, G. H.; Li, D. J.; Li, Q. H.; Zhang, L.; Zhang, J. Combining a titanium-organic cage and a hydrogen-bonded organic cage for highly effective third-order nonlinear optics. *Angew. Chem. Int. Ed.* **2021**, 60, 2920–2923.

(26) Chen, G. H.; Li, D. J.; He, Y. P.; Zhang, S. H.; Liang, F. P.; Zhang, J. Self-assembly of a $Ti_4(embonate)_6$ cage toward silver. *Inorg. Chem*. **2020**,

DOI: 10.14102/j.cnki.0254-5861.2021-0016

59, 14861–14865.

(27) Chen, G. H.; Li, H. Z.; He, Y. P.; Zhang, S. H.; Yi, X.; Liang, F. P.; Zhang, L.; Zhang, J. Ti_4(embonate)$_6$ based cage-cluster construction in a stable metal-organic framework for gas sorption and separation. *Cryst. Growth Des*. **2019**, 20, 29–32.

(28) Gan, D. E.; Zhang, Z.; Li, Q. H.; Li, W. M. Oligo(aromatic ether sulfone)-F as a nonlinear polarized polymeric material: an experiment and DFT study. *Chin. J. Struct. Chem*. **2021**, 40, 383–393.

Received: October 28, 2021
Accepted: November 19, 2021
Published: January 13, 2022

DOI: 10.14102/j.cnki.0254-5861.2021-0016